Catalysis Today xxx (2016) xxx–xxx

Contents lists available at ScienceDirect

Catalysis Today

journal homepage: www.elsevier.com/locate/cattod

Microfibrous entrapped hybrid iron-based catalysts for Fischer–Tropsch synthesis

Xinquan Cheng[a], Hongyun Yang[b], Bruce J. Tatarchuk[a,*]

[a] Center for Microfibrous Materials, Department of Chemical Engineering, 212 Ross Hall, Auburn University, AL 36849, USA
[b] IntraMicron Inc., 368 Industry Dr., Auburn, AL 36832, USA

ARTICLE INFO

Article history:
Received 13 December 2015
Received in revised form 25 February 2016
Accepted 28 February 2016
Available online xxx

Keywords:
Microfibrous entrapped catalysts
Fischer–Tropsch synthesis (FTS)
Hydrocracking
Supported Fe-based FTS catalyst
Hybrid catalyst
Mesoporous aluminosilicate

ABSTRACT

Fischer–Tropsch synthesis (FTS) is a highly exothermic reaction, and a FTS reactor must have an efficient heat transfer mechanism in order to maintain a stable reaction temperature. Copper microfibrous entrapped catalyst (Cu MFEC) has demonstrated an excellent intra-bed heat transfer ability for FTS thermal management. The porous structure of Cu MFEC can entrap any pre-manufactured catalyst particles, while its counterpart approaches such as metallic foams or monolith reactor structures are typically based on washcoating process and require the details about catalyst formulation and preparation procedure to proceed. In this investigation, a highly active and stable iron-based FTS (Fe-FTS) catalyst, i.e. iron supported on γ-alumina and promoted with copper and potassium, has been developed. The apparent reaction rate constant of Fe-FTS and its productivity at 27.7% of CO conversion are 167 mmol $(H_2 + CO)/g_{cat}$/h and 0.30 gC_5+/g_{cat}/h, respectively, which are comparable to the most active unsupported Fe-based catalyst. When Fe-FTS was physically mixed with equal mass of mesoporous aluminosilicate (MAS) loaded with 0.3 wt% Pt, a hybrid catalyst was formed. This hybrid catalyst demonstrated an extremely low CO_2 selectivity (27.7 C%) and a very high selectivity (38.1 C%) to liquid products (C_5–C_{20}). The result suggested that FTS and hydrocracking process simultaneously took place within a single reactor. Furthermore, FTS was carried out in a larger tubular reactor (34.0 mm I.D.) packed with Cu MFEC. It demonstrated a radial temperature gradient less than 5 °C and similar reactivity and product selectivity as those obtained in a small FTS reactor (9.5 mm I.D.). While with the same catalyst loading density and the same test conditions, the comparative packed bed (34.0 mm I.D.) reached radial temperature gradient around 54 °C. It was also found that the FTS based Cu MFEC required negligible amount of time to reach its steady state compared with the packed bed. With these attributes and advantages, Cu MFEC approach is a promising alternative to the traditional packed bed for exothermic reactions such as FTS.

1. Introduction

Fischer–Tropsch synthesis (FTS) is a well-known Gas-to-Liquid technique for converting natural gas or syngas into liquid fuels. However, FTS is a highly exothermic reaction which causes many heat transfer issues for FTS intensification since FTS was established in 1920s [1]. First of all, the reaction temperature is easy to run away due to extensive heat generation, which can lead to some severe quality and even safety problems. More importantly, FTS is a temperature sensitive reaction, and its product distribution is strongly dependent on the reaction temperature. Undesirable gaseous products like methane, ethane, etc. will be produced at high temperatures. For the maximum selectivity to desired liquid products, the FTS reactor should be well controlled at a single stable temperature for entire reactor. In addition, the high reaction temperature could deactivate the catalysts by sintering its active metal sites. As a result, an efficient heat transfer is the key to solve FTS related issues.

In the past, researchers put tremendous efforts to develop various heat transfer structures for FTS in order to avoid reaction temperature overshoot and formation of hot spots. The major representative works are fluidized reactor and slurry reactor. Both of them have been successfully used in research and industrial areas [2–7]. For other types of reactors, including metallic foams and metal monolith catalyst structures, some successful applications also existed in their infant stage [8–12]. However, they all have disadvantages. For instance, fluidized reactors require catalysts with good mechanical strength and complicated downstream

* Corresponding author.
E-mail address: tatarbj@auburn.edu (B.J. Tatarchuk).

http://dx.doi.org/10.1016/j.cattod.2016.02.048
0920-5861/

recovery processes [3]. The serious issues for slurry reactor are back-mixing of the gas phase, catalyst attrition and separation from the liquid and wax products [13]. For metallic foams and monolith reactor structures, catalysts need to be prepared either directly on the reactor structure or on a washcoating process to load catalytic components [14,15]. Hence, these two kinds of reactor structures are not suitable for pre-manufactured catalysts. Through persistent efforts, our group developed a novel catalyst structure called microfibrous entrapped catalyst (MFEC) structure which is now commercially available at IntraMicron Inc. MFEC is a structured catalyst and it consist of a highly porous network structure made of micron-sized metal, glass, or polymer fibers with small catalyst particles entrapped inside [16–20]. One of the biggest advantages of MFEC when compared with metallic foams or monolith reactor structures is that MFEC can be used for pre-manufactured catalyst particles. This unique advantage greatly extends the applications of MFEC on many heterogeneous reactions by using the original optimized catalyst recipes, instead of seeking a new recipe for washcoating support [21–23]. Previous efforts have found out that MFEC demonstrates high void volume, which significantly reduces pressure drop compared with packed bed. Moreover, intra-particle heat transfer and mass transfer are enhanced in MFEC structure, since small particles are used and acceptable uniform particle distribution are achieved. This unique catalyst structure have been widely used in various fields. For instance, Yang et al. studied the effects of microfibrous media on external mass transfer in desulfurization [24,25]. Zhu et al. discussed the electrical conductivity of metal microfibrous in fuel cell [26,27]. Gu et al. built a Computational Fluid Dynamics pressure drop model for MFEC filter [28]. Sheng et al. investigated and simulated the thermal properties of MFEC and applied to FTS reaction [29–31]. According to Sheng et al.'s investigation, copper MFEC can significantly enhance intra-bed heat transfer and maintain a stable reaction temperature for highly exothermic reaction like FTS.

FTS produces a broad spectrum of products including gas, liquid and wax [32,33]. In order to maximize amount of hydrocarbons in the range of liquid fuels, a suitable operational conditions are required. For example, cobalt based catalyst typically requires 220 °C and 20 bar to produce hydrocarbon liquids with the maximum selectivity. In order to further enhance hydrocarbon liquid fraction, paraffinic wax formed during FTS is hydrocracked to form more liquids. Traditionally, the complicated and expensive process of hydrocracking is performed downstream in a separate reactor. However, by physical mixing of an FTS catalyst with an acidic zeolite component, the FTS and hydrocracking process can simultaneously occur in a single reactor [34–36]. The common FTS catalysts used in the industry are cobalt and iron based catalysts [37,38]. Iron-based catalysts are more favorable to produce long chain hydrocarbons from coal or biomass (low H_2/CO ratio) due to their high water-gas shift activity, low cost and low methane selectivity [5]. Typically, unsupported iron catalysts promoted with copper and potassium are used in the industry. These catalysts provide high activity and selectivity to hydrocarbons. However, the unsupported Fe-based catalysts are generally lack of physical strength and durability. In contrast, alumina-supported Fe-based catalysts although providing low activity and high methane selectivity, are stronger and more attrition resistant than unsupported Fe-based catalysts [39].

In the current investigation, a highly active and stable γ-alumina supported Fe-based catalyst was prepared and tested for FTS, and a mesoporous aluminosilicate (MAS) was synthesized as hydrocracking catalyst. A hybrid FTS catalyst that physically combined these two components together, has been developed to be applied on FTS and hydrocracking reactions simultaneously within a single reactor. The results revealed that this type of hybrid catalyst can produce wax-free liquid fuels (C_{23}+ less than 5 wt%), but the C_5–C_{20} selectivity was relative low and the selectivity of light hydrocarbons (C_1–C_4) was significantly high. Recently, the addition of 0.3 wt% of Pt to the MAS for formation of a new hybrid FTS catalyst greatly enhanced C_5–C_{20} selectivity and reduced the selectivities to CO_2 and the light hydrocarbons (C_1–C_4).

Typical tubular reactors filled of active FTS catalysts will experience thermal runaway at a large reactor diameter due to inefficient radial heat transfer through the packed bed. However, the Cu MFEC structure successfully scaled up the FTS reaction to this larger degree without losing catalyst activity and major product selectivity, by significantly enhancing heat transfer and maintaining a stable reaction temperature. In order to demonstrate the benefits of the MFEC structure, a tubular reactor with a large inside diameter (I.D.) of 34.0 mm I.D. has been designed and tested for FTS using hybrid FTS catalysts.

2. Experimental

2.1. MFEC structure and catalyst preparation

2.1.1. Fabrication of Cu MFEC

A traditional paper-making technique was developed to prepare MFEC by Auburn University. The detailed process can be found in the literature [31]. Briefly, micro-sized copper fibers and cellulose fibers were dispersed in an aqueous suspension. Then, the resulting mixture was cast into a paper-making model and formed a preformed sheet by removing the water. A two-sided sheet can be fabricated by stacking two pieces of performed sheets together, which were made by copper microfibers with different diameters. The top layer was made by 12 μm diameter copper microfibers, and the bottom layer was 4 μm diameter copper microfibers (IntraMicron, Auburn, AL, USA). After drying these two layers, a self-supporting two-sided sheet has been created. Subsequently, this preformed sheet was pre-oxidized in a flowing air at 500 °C for 30 min in order to remove the bulk of cellulose. Then, the pre-oxidized sheet was sintered in a flow of hydrogen at 700 °C for 60 min to form fiber-fiber junctions. These junctions can form a sinter-locked network through the fiber media, which greatly enhanced heat transfer on this media. The final step was loading catalyst particles with certain sizes into this porous microfiber media. Actually, after sintering, the top layer of media became very fluffy, and bottom layer was much compact since it was made by fibers with smaller diameter. Hence, the catalyst particles can be easily load into the top layer of this microfiber media, and the bottom layer was aimed to prevent the catalyst particles from leaking or moving out from the microfiber media.

2.1.2. Preparation of Fe-based FTS catalyst

The Fe-based FTS catalyst was supported on a commercial grammar-alumina (Alfa Aesar, γ-Al_2O_3 #43832). The metal precursors were iron(III) nitrate nonahydrate (Alfa Aesar, ACS grade, 98.0–101.0 wt%), copper(II) nitrate hemipentahydrate (Alfa Aesar, ACS grade, 98.0–102.0 wt%), and potassium hydrogen carbonate (Alfa Aesar, ACS grade, 99.7–100.5 wt% dried basis). In a typical procedure, γ-Al_2O_3 were grounded and sieved to 60–80 mesh (177–250 μm), and then calcined in static air at 750 °C for 5 h to remove the hydroxyl groups on the surface. Then, 9.3 g $Al(NO_3)_3{\cdot}9H_2O$, 2.555 g $Cu(NO_3)_3{\cdot}2.5H_2O$, and 0.954 g $KHCO_3$ were dissolved in 36.0 mL deionized water. An excess solution impregnation method was used to load the metal solution on 3.0 g calcined γ-Al_2O_3 in three steps [40,41]. In each step, one third of the above metal solution was added to the support while kept it on a shaker and dried it slowly in atmosphere. After drying, the sample was calcined at 300 °C for 5 h in static air. Then, the previous steps were repeated two times in order to load the leftover metal solution. It must be noted that each time of loading followed by calcination.

Please cite this article in press as: X. Cheng, et al., Microfibrous entrapped hybrid iron-based catalysts for Fischer–Tropsch synthesis, Catal. Today (2016), http://dx.doi.org/10.1016/j.cattod.2016.02.048

Finally, an iron-based FTS catalyst with a nominal compositions of 100Fe/7.5Cu/4K/233Al_2O_3 (mass basis) was fabricated and was named as Fe-FTS.

2.1.3. Synthesis of MAS and Pt-MAS

A sol-gel synthetic method was used to synthesize this mesoporous aluminosilicate (MAS) [42]. Aluminum nitrate nonahydrate (ANN, J.T. Baker, ACS grade, 98.7 wt%) and tetraethylorthosilicate (TEOS, Alfa Aesar, 99.9 wt%) were used as the alumina and silica source, respectively. Cetyltrimethyl ammonium bromide (CTAB, Spectrum Chemical MFG. Corp., 98–101 wt%) was used as the templating agent. Also, ammonium hydroxide (NH_4OH, BDH Chemicals, 30 wt%) and ethyl alcohol (C_2H_5OH, EMD Chemicals Inc., ACS grade, 99.5 wt%) were presented. The molar composition of the synthesis mixture was as followed: 1.0 TEOS:0.13ANN:40H_2O:8C_2H_5OH:0.25CTAB:10NH_4OH. In a typical synthesis, 4.88 g ANN was dissolved in 46.7 mL C_2H_5OH and then mixed with 22.3 mL TEOS. Meanwhile, 9.1 g CTAB, 72.0 mL water, and 116.8 g NH_4OH solution were mixed together under constant stirring. After 30 min, the TEOS solution was added to the CTAB mixtures drop by drop while keeping stirring. After all the solution has been added, the mixture was increased to and kept at 60 °C under stirring for 3 days. The resulting gel was filtered and washed with an excess amount of water to remove unreacted components. After drying overnight at 100 °C, the resulting sample was calcined at 540 °C for 6 h in order to remove the template.

An incipient wetness impregnation method has been applied to prepare 0.3 wt% Pt-MAS by using tetraammineplatinum(II) nitrate (Alfa Aesar, ACS grade, 99 wt%) as the Pt source. After drying at 120 °C for 6 h, the sample was calcined at 500 °C for 4 h in static air.

2.1.4. Preparation of hybrid catalysts

Hybrid catalysts were composed with two parts. One part is the FTS catalyst mentioned above, Fe-based catalyst (Fe-FTS), with a nominal compositions of 100Fe/7.5Cu/4K/233Al_2O_3 (based on mass). The other part is the hydrocracking catalyst which is ZSM-5 (Zeolyst, CBV 8014, Si/Al = 80:1), or MAS, or Pt-MAS. In a typical process, a physical powder mixture of 50 wt% Fe-FTS catalyst and 50 wt% hydrocracking catalyst was pressed into extrudate form, and then the extrudates were crushed and separated to 60–80 mesh particles. The resulted hybrid catalysts were named as Fe-FTS/ZSM-5, Fe-FTS/MAS and Fe-FTS/Pt-MAS for the aforementioned three hydrocracking catalysts, respectively. It is worth to know that the ZSM-5 was activated at 540 °C for 3 h before using.

2.2. Catalyst characterization

Nitrogen adsorption/desorption isotherms were recorded at −196 °C on a Micromeritics TriStar II 3020 instrument. Before the measurement, samples were degassed at 200 °C under N_2 flow overnight. The total surface areas of samples were calculated via the Brunauer–Emmett–Teller (BET) equation. Average pore diameter and pore size distribution were calculated by using Barrett–Joyner–Halenda (BJH) method. The surface morphologies of Cu MFEC structure before and after catalyst loading were characterized on a JEOL JSM-7000F scanning electron microscope (SEM).

2.3. FTS reaction measurements

2.3.1. Packed bed

All the FTS experiments in this paper can be separated into two groups. One tested FTS catalysts in packed beds and the other evaluated these catalysts in the Cu MFEC structure. For packed bed tests, usually 0.5 g of Fe-FTS catalyst (60–80 mesh) was diluted with certain amount of glass beads (Alfa Aesar, acid washed, 60–80 mesh). When it turns to hybrid catalyst, 1.0 g of hybrid catalysts were used for the reaction in order to keep the Fe-based FTS catalyst in the same amount. Before applying the FTS reaction, the catalysts were pre-reduced in situ at 120 °C for 2 h under flow of ultra-high purity hydrogen (Airgas, HY UHP300, 99.999%), then the temperature was slowly increased to 280 °C for another 10 h, followed by gradually rose up the temperature to 320 °C for another 4 h. Then, the catalysts were cooled down to 260 °C to initiate the FTS reaction. All the experiments in this paper were carried out at 260 °C and 2.0 MPa by using a syngas with H_2/CO ratio equals of 2:1. This syngas was directly purchased from Airgas with 1.5 vol% nitrogen as the internal standard. The outlet stream went sequentially through a hot trap (150 °C) and a cold trap (2 °C) to collect heavy hydrocarbons and liquid products, respectively. The residual gas products were analyzed on an online gas chromatograph (GC, Agilent 6890) equipped with a packed column (Hayesep-DB 100/120). A thermal conductivity detector (TCD) was used to determine the concentrations of CO, CO_2, and C_1–C_6 using nitrogen as the internal standard. In the same GC, there was a capillary column (DB-5) connected with a flame ionization detector (FID) which was used to analyze liquid and wax products. The collected wax products were dissolved and diluted in carbon disulfide (Alfa Aesar, ACS grade, >99.9 wt%) and then shot into the FID.

Table 1
Nitrogen sorption data.

Sample	BET Surface Area (m^2/g)	Pore Volume (cm^3/g)	Average Pore Diameter (nm)
Calcined γ-Al_2O_3	216	0.75	11.7
Fe-FTS	74	0.25	10.7
MAS	1108	1.00	3.5
Pt-MAS	1061	0.95	3.5
ZSM-5[a]	450	0.27	0.56

[a] The sorption data of ZSM-5 was referenced from the literatures [45,46].

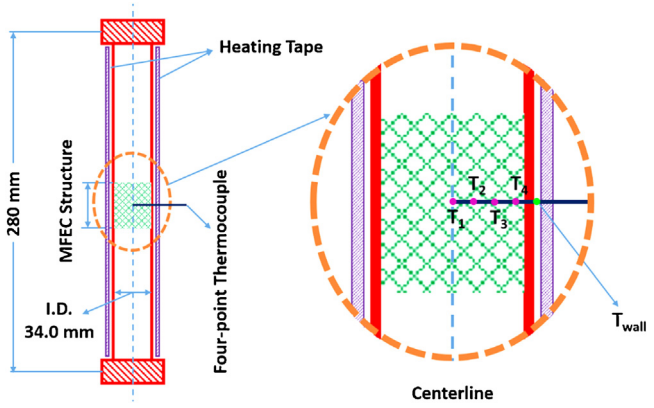

Fig. 1. The Cu MFEC reactor structure (From T_1 to T_4, the intervals between each point are 10.0 mm, 2.0 mm and 5.0 mm, respectively. T_{wall} is the outside reactor temperature).

2.3.2. Cu MFEC structure

The Cu MFEC structure was only used in the large reactor (34.0 mm I.D.). First, the calcined catalyst particles were entrapped into a sintered copper microfiber media to form a Cu MFEC structure. Secondly, circular disks with a diameter of 36.0 mm was punched out from the Cu MFEC to packing into the tubular reactor. The disk size (36.0 mm) were 6% larger than the inside diameter of the tubular reactor (34.0 mm), which can offer tremendous contact points between the copper fiber media and the reactor wall. By doing this, the inside wall heat transfer coefficient increased significantly when compared with the traditional packed bed. As shown in Fig. 1, a four-point thermocouple was inserted into the

Please cite this article in press as: X. Cheng, et al., Microfibrous entrapped hybrid iron-based catalysts for Fischer–Tropsch synthesis, Catal. Today (2016), http://dx.doi.org/10.1016/j.cattod.2016.02.048

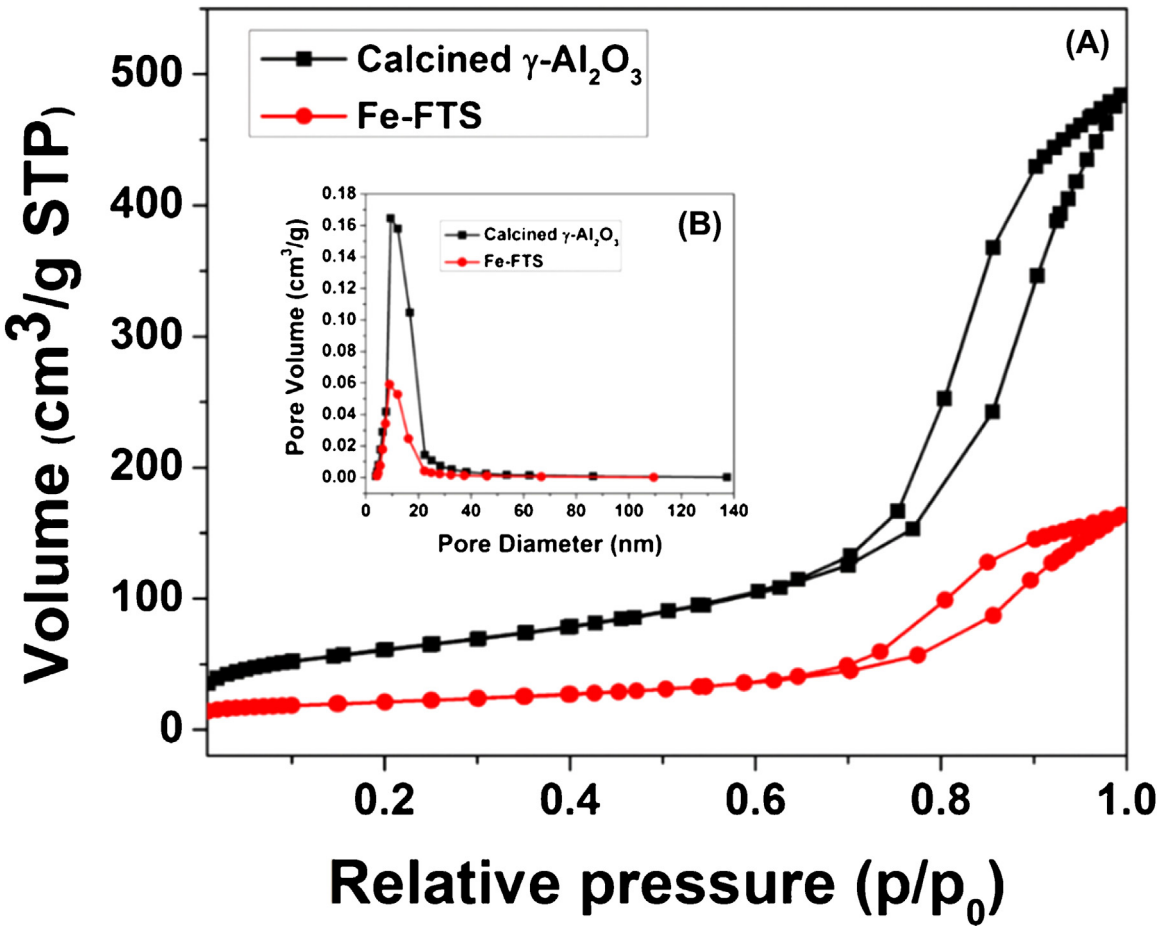

Fig. 2. N_2 sorption data (A) adsorption/desorption isotherms of calcined γ-Al_2O_3 and Fe-FTS; (B) pore size distribution patterns of calcined γ-Al_2O_3 and Fe-FTS.

Table 2
Performance of different catalysts in both packed bed and Cu MFEC structure.

Reactor size[a]	I.D. 9.5 mm				I.D. 34.0 mm			
Reactor structure[b]	PB				MFEC	MFEC	MFEC	PB
Experiment number[c]	SR-1	SR-2	SR-3	SR-4	LR-1	LR-2	LR-3	LR-4
Catalyst composition[d]	Fe-FTS	Fe-FTS/ZSM-5	Fe-FTS/MAS	Fe-FTS/Pt-MAS	Fe-FTS	Fe-FTS	Fe-FTS/Pt-MAS	Fe-FTS
Voidage, %	43.9	39.0	33.3	33.4	65.6	64.6	44.8	45.3
HSGV, Nl/g_{Fe}/h	5.7	5.7	5.7	5.7	5.7	3.3	3.3	5.7
Time on stream, h	120	120	96	96	60	60	60	60
CO conversion, %	27.7	30.1	33.2	25.7	18.5	24.2	18.1	50.4
Rate constant[e]	167	181	231	186	143	108	94	284
Product selectivity, C%								
CO_2	41.3	36.4	31.1	27.7	37.3	40.3	24.3	44.7
CH_4	5.2	9.9	16.0	12.3	7.9	8.7	10.8	8.3
C_2–C_4	16.7	22.9	31.9	19.9	19.2	22.6	23.4	20.6
C_5–C_{20}	29.4	29.3	20.6	38.1	28.8	22.8	39.0	24.6
C_{21}+	7.4	1.5	0.4	2.0	6.8	5.6	2.5	1.8
Catalyst productivity[f]	0.30	0.28	0.22	0.32	0.21	0.14	0.18	0.40
α value[g]	0.81	–	–	–	0.80	0.76	–	0.79
H_2O/oil mass ratio[h]	1.0	1.9	7.0	4.1	1.0	1.0	3.6	0.8

All the experiments in this table were carried out at 260 °C and 2.0 MPa by using a syngas with H_2/CO ratio equals to 2:1

[a] Two kinds of tubular reactor were used, their inside diameter are 9.5 mm and 34.0 mm, respectively.

[b] PB means packed bed and MFEC means copper MFEC structure.

[c] The experiments operated on the small reactor (9.5 mm I.D.) named as SR- and on the large reactor (34.0 mm) named as LR-.

[d] Four kinds of catalysts were used, Fe-FTS is only for Fischer–Tropsch reaction and hybrid catalysts were fabricated from Fe-FTS by physically mixed with ZSM-5, or MAS, or Pt-MAS.

[e] Apparent reaction rate constant means mmol $(H_2 + CO)/g_{cat}$/h. For hybrid catalyst, g_{cat} means per gram of Fe-FTS without counting the equal mass of hydrocracking catalyst.

[f] Catalyst productivity means g C_5+/g_{cat}/h and g_{cat} still means the weight of Fe-FTS catalyst for hybrid catalysts.

[g] Calculated by using ASF equation (Figs. S1–S4, Supporting information).

[h] The mass ratio of collected water to oil phase.

Please cite this article in press as: X. Cheng, et al., Microfibrous entrapped hybrid iron-based catalysts for Fischer–Tropsch synthesis, Catal. Today (2016), http://dx.doi.org/10.1016/j.cattod.2016.02.048

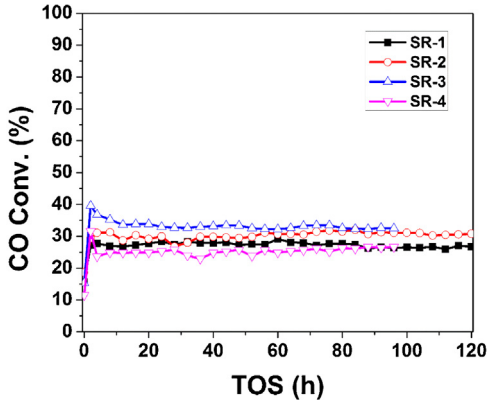

Fig. 3. CO conversion vs. time on stream for four experiments carried out in the small reactor: SR-1 for Fe-FTS; SR-2 for Fe-FTS/ZSM-5; SR-3 for Fe-FTS/MAS; SR-4 for Fe-FTS/Pt-MAS (solid dot for FTS catalyst and empty dot for hybrid catalysts).

reactor from the outside wall of the reactor wall when the reactor was loaded in the half-way, and then the other half of the bed was loaded. In that way, the radial temperature distribution profiles can be measured precisely. For Cu MFEC structures, all the reaction conditions and product analysis system were the same with the above mentioned packed bed.

3. Results and discussion

3.1. Catalyst activity and selectivity

3.1.1. Small reactor for catalyst screening

Fe-FTS is an iron-based FTS catalyst that is supported on calcined γ-alumina and promoted with copper and potassium. The porous structures of alumina support and Fe-FTS have been measured by N_2 sorption (Fig. 2). As shown in Table 1, after metals loading, the support's BET surface area was significantly decreased from 216 to 74 m^2/g, and the pore volume was also drastically reduced from 0.75 to 0.25 cm^3/g due to the very high iron loading ratio (30 wt%). The average pore diameter was slightly decreased from 11.7 to 10.7 nm (Table 1). The Fe-FTS catalyst was tested in a small tubular reactor (9.5 mm I.D.) under a typical FTS reaction condition (260 °C, 2.0 MPa, and H_2/CO = 2:1). At a CO conversion of 27.7% (SR-1 in Table 2), the apparent reaction rate constant of Fe-FTS was 167 mmol (H_2 + CO)/g_{cat}/h and the corresponding productivity was 0.30 gC_5+/g_{cat}/h. These values are higher than those obtained on typical supported Fe-based catalysts and comparable to those achieved on most active unsupported Fe-based catalysts [43]. In addition, the selectivity to methane was very low (5.2 C%) and a high α value (0.81) was calculated by following the Anderson-Schulz-Flory distribution (Fig. S1, Supporting information). Although the selectivity of CO_2 was very high, which is a common phenomenon for Fe-based FTS catalyst because of the water-gas shift reaction [44]. Furthermore, the Fe-FTS catalyst was very stable and no catalyst deactivation was observed during the 120 h of operation (Fig. 3). Therefore, Fe-FTS is a highly active and stable γ-alumina supported Fe-based FTS catalyst.

One of the major reasons for this high activity is that the alumina support was pretreated at 750 °C for 5 h before loading metals in order to remove the hydroxyl groups on the surface. Decreasing the surface hydroxyl groups can reduce the formation of $FeO{\cdot}Al_2O_3$ surface spinel, which cannot be reduced to the FTS active species under the typical reduction conditions [39]. Moreover, this Fe-based FTS catalyst had very high iron loading (30 wt%) and was promoted by copper and potassium. It is well known that Cu promoter facilitates the dispersion and reduction of iron species, and potassium promoter enhances the CO adsorption and carburization. All these facts contributed to this high reaction activity and high productivity. Apparently, supported Fe-based catalyst owns many advantages than unsupported ones under a similar reaction activity and product selectivity [39].

Based on this highly active and stable Fe-based FTS catalyst (Fe-FTS), three hybrid catalysts were prepared by physically mixing Fe-FTS with ZSM-5, MAS, and Pt-MAS, and were named as Fe-FTS/ZSM-5, Fe-FTS/MAS, and Fe-FTS/Pt-MAS, respectively. The corresponding experiments were named as SR-2, SR-3, and SR-4, respectively. All the experiments (from SR-1 to SR-4) in the small reactor (9.5 mm I.D.) were operated at the same reaction conditions, and the reaction activities and selectivities of these catalysts were obtained at similar CO conversion levels of 26–33%. Hence, the measured values of activity and selectivity for these catalysts are directly comparable. As shown in Table 2, all the hybrid catalyst demonstrated much different product distributions compared with that of plain Fe-FTS catalyst. Due to the hydrocracking activity of ZSM-5 [47], the hybrid catalyst Fe-FTS/ZSM-5 (SR-2 in Table 2) demonstrated a high selectivity of 32.8 C% to light chain hydrocarbons (C_1–C_4) a low selectivity of 1.5 C% to C_{21}+, compared with those obtained by Fe-FTS at 21.9 C% and 7.4 C%, respectively (SR-1 in Table 2). Because the decreased selectivity to C_{21}+, the catalyst production rate to C_5+ slightly decreased from 0.3 to 0.28 gC_5+/g_{cat}/h, even at higher reaction rate and higher CO conversion. In addition, the liquid product selectivity (C_5–C_{20}) in SR-2 was almost the same as that in SR-1. Therefore, Fe-FTS/ZSM-5 is not an ideal hybrid catalyst for liquid hydrocarbon production.

According to the literature [46], hydrocracking selectivity to long chain hydrocarbons can be improved significantly if the pore size of hydrocracking catalyst can reach mesoporous range. Considering about this, a mesoporous aluminosilicate (MAS) with a larger pore size (3.5 nm) was synthesized as the hydrocracking catalyst. The N_2 adsorption/desorption isotherm shown the presence of a H2 hysteresis loop with an abrupt step around P/P_0 = 0.52 in the desorption branch of MAS (Fig. 4A). This is a typical mesoporous adsorption and desorption isotherm. As shown in Fig. 3B, MAS has a narrow pore size distribution, and the average pore diameter is 3.5 nm. Moreover, MAS has a very high surface area (1108 m^2/g) and its pore volume reach of 1.00 cm^3/g (Table 1). Therefore, MAS could be an excellent candidate as a hydrocracking catalyst and the experimental results confirmed this expectation. Hybrid catalyst Fe-FTS/MAS (SR-3 in Table 2) significantly rose up the selectivity of C_1–C_4 to 47.9 C%, and reduced the C_5–C_{20} selectivity to 20.6 C%. Moreover, the catalyst productivity dropped to 0.22 gC_5+/g_{cat}/h. This is due to the large pore size of MAS can fit in the long chain hydrocarbons, which greatly increased the chance of heavy products to get hydrocracked to short chain hydrocarbons. These results also suggest Fe-FTS/MAS is not a suitable catalyst for the selective production of FTS liquids.

It must be noted that the CO_2 selectivity in SR-3 decreased to 31.1 C% which is much less than the CO_2 selectivity in SR-1 (41.3 C%). One possible reason is that the acid components of MAS provided active protons (H^+) to terminate the active oxygen (O^{2-}) that dissociated from CO or H_2O, which suppressed the formation of CO_2 [48]. If this assumption is right, the production of H_2O should be increased. In order to prove that, the mass ratio of H_2O to liquid oils has been calculated. The results shown that the mass ratio of H_2O/oil was around 1.0 for Fe-FTS catalyst (SR-1), but it increased to 1.9 when hybrid catalyst Fe-FTS/ZSM-5 was used (SR-2 in Table 2). The mass ratio further rose up to 7.0 when hybrid catalyst Fe-FTS/MAS (SR-3 in Table 2) was used. This is an extremely high H_2O/oil mass ratio and the very low C_5+ selectivity (21.0 C%) made a part of the contribution. These results verified our argument that acid component can suppress water-gas shift reaction activity and promote water production.

Please cite this article in press as: X. Cheng, et al., Microfibrous entrapped hybrid iron-based catalysts for Fischer–Tropsch synthesis, Catal. Today (2016), http://dx.doi.org/10.1016/j.cattod.2016.02.048

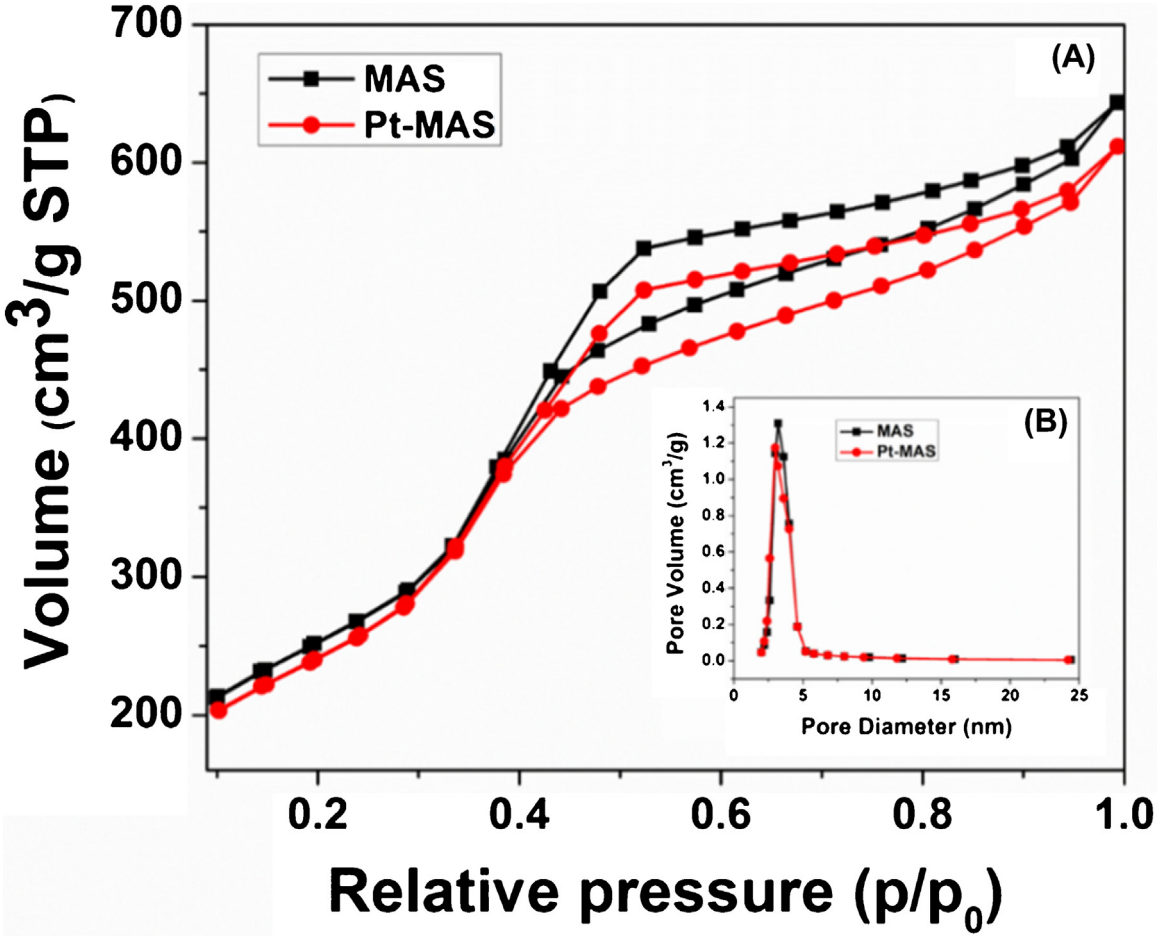

Fig. 4. N_2 sorption data (A) adsorption/desorption isotherms of MAS and Pt-MAS; (B) pore size distribution patterns of MAS and Pt-MAS.

Because monofunctional cracking catalysts, e.g. MAS usually produce mostly of short and unsaturated hydrocarbons, Fe-FTS/MAS is not an ideal hybrid catalyst for the maximum production of liquid hydrocarbons. In contrast, bifunctional hydrocracking catalysts can maximize the production of middle distillates by making a balance between the acid and the metal functions [49,50]. Typically, noble metals such as Pt or Pd are used to build bifunctional hydrocracking catalysts due to their higher hydrogenating activity. This property can improve the yield of middle distillates as well as reduce the light hydrocarbons formation. In addition, a strong hydrogenation function can enhance catalyst stability through suppressing the formation of coke precursors [51].

In light of the aforementioned fundamentals, 0.3 wt% of Pt was loaded on MAS to form a bifunctional hydrocracking catalyst (Pt-MAS). The texture property of Pt-MAS was characterized by N_2 sorption (Table 1). When compared with MAS, the BET surface area of Pt-MAS slightly decreased to 1061 m^2/g and its pore volume also slightly reduced to 0.95 cm^3/g, but its average pore diameter almost remained unchanged since Pt loading content was very low. The hybrid catalyst Fe-FTS/Pt-MAS was tested for FTS performance (SR-4 in Table 2). The result showed that the C_1–C_4 selectivity and CO_2 selectivity of Fe-FTS/Pt-MAS were 32.2 C% and 27.7 C%, respectively, which are much lower than those achieved by Fe-FTS/MAS, 47.9 C% and 31.1 C%, respectively. Its C_5–C_{20} selectivity reached 38.1 C%, which is much higher than that of Fe-FTS/MAS (20.6 C%) and is the highest among all three hybrid catalyst selective to liquid fraction. Moreover, the catalyst productivity was increased to 0.32 $gC_5+/g_{cat}/h$ even at a slightly lower CO conversion. In a word, Fe-FTS/Pt-MAS is a good hybrid catalyst formulation for the maximum liquid hydrocarbon production compared with the hybrid catalyst with ZSM-5 and MAS. Therefore, the best hybrid catalyst has been screened out and can be used for further study in Cu MFEC structure.

3.1.2. *Large reactor for Cu MFEC structure*

In the catalyst screening step, all the evaluations were performed in a small tubular reactor (9.5 mm I.D.). Since the Cu MFEC structure can greatly enhance radial heat transfer, a larger reactor could demonstrate this benefit more remarkable. Therefore, a much larger tubular reactor with 34.0 mm I.D. was used to construct the Cu MFEC reactor. Fig. 5A showed the picture of copper microfiber media which has a very fluffy structure at the top layer, hence catalyst particles can easily migrate into the fiber media by utilizing a shaker and resulting acceptable dispersion (Fig. 5C). After loading, the catalyst particles were immobilized by the sintered microfiber network (Fig. 5D), and the compacted bottom layer prevented the loss of catalyst particles. In addition, the Cu MEFC media were stacked up tightly during the time of packing in order to enhance axial heat transfer. Therefore, catalysts entrapped in MFEC structure are immobilized even under a high space velocity.

The first experiment (LR-1 in Table 2) was used to compare with SR-1 by keeping all the reaction conditions as the same. The results show that both the apparent reaction rate constant and the catalyst productivity of LR-1 were decreased when compared with SR-1. This is mainly because of the CO conversion in LR-1 (18.5%) was much lower than the CO conversion in SR-1 (27.7%). If the differences in CO conversion have been corrected, the reaction activity (apparent rate constant and catalyst productivity) of LR-1 would

Please cite this article in press as: X. Cheng, et al., Microfibrous entrapped hybrid iron-based catalysts for Fischer–Tropsch synthesis, Catal. Today (2016), http://dx.doi.org/10.1016/j.cattod.2016.02.048

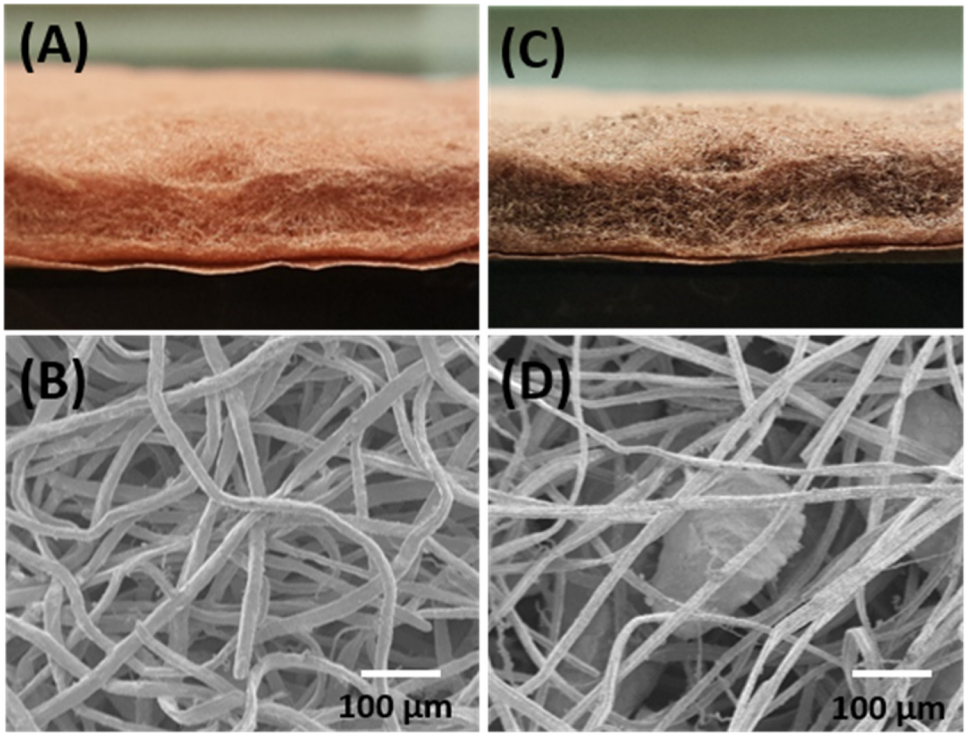

Fig. 5. Images of Cu MFEC structure: (A) Picture of Cu MFEC before catalyst loading; (B) SEM image of Cu MFEC before catalyst loading; (C) Picture of Cu MFEC after catalyst loading; (D) SEM image of Cu MFEC after catalyst loading.

be higher than the reaction activity of SR-1. In LR-1, the product selectivities were similar with SR-1. Moreover, αvalue in LR-1 was 0.80 (Fig. S2, Supporting information) which is also similar with α value in SR-1 (0.81). In conclusion, copper microfibrous entrapment enable the high exothermic reaction taking place in a tubular reactor with a large reactor diameter without compromising the reaction activity and product selectivity.

In order to fairly compare the performance of MFEC with the catalysts tested in small packed bed, the CO conversion should be kept at a similar level. Hence, more catalyst was loaded into the Cu MEFC structure and the space velocity was also decreased. By holding other reaction conditions unchanged, the CO conversion in LR-2 was increased to 24.2%, which is comparable to the CO conversion (27.7%) in SR-1. Compared with LR-1, the apparent reaction rate constant in LR-2 decreased to 108 mmol $(H_2 + CO)/g_{cat}/h$ and the productivity dropped to 0.14 $gC_5+/g_{cat}/h$. This does not mean reduced the reaction activity, since more catalyst has been loaded and lower syngas was pass through the reactor. Meanwhile, the C_5–C_{20} selectivity reduced to 22.8 C%, and the selectivity of C_1–C_4 and CO_2 slightly increased to 31.3 C% and 40.3 C%, respectively.

Under the same reaction conditions of LR-2, the Cu MFEC structure entrapped with hybrid catalyst Fe-FTS/Pt-MAS (LR-3 in Table 2) was tested in order to compare the FTS performance of SR-4. As a result, both the apparent reaction rate constant and the catalyst productivity decreased when compared with SR-4. However, LR-3 had the highest C_5–C_{20} selectivity (39.0 C%) and the lowest CO_2 selectivity (24.3 C%). Meanwhile, the selectivity of C_1–C_4 in LR-3 was similar to that in SR-4. Hence, the SR-4 has been scaled up on a large Cu MFEC reactor (34.0 mm I.D.) without apparent losing reaction activity and desired product selectivity.

It must be pointed out that, under the same reaction conditions, CO conversion in LR-1 was lower than in SR-1 due to the impact of Cu MFEC structure. Cu MFEC structure can highly efficient transfer the reaction heat out of the reactor and avoid temperature overshoot or the formation of hot spots. This implied that LR-1 operated at a relatively lower temperature than SR-1, which led to a lower CO conversion. For a comparison purpose, a packed bed was loaded (LR-4 in Table 2) by using α-Al_2O_3 to dilute the bed to the same degree as LR-1 and kept all the other reaction conditions unchanged. It turns out that the CO conversion in LR-4 (50.4%) was much higher than in LR-1 (18.5%), but with a relatively lower C_5–C_{20} selectivity and higher CO_2 selectivity. This is mainly caused by the very poor heat transfer ability of packed bed, which led to serious temperature overshooting and increased the CO conversion. As shown in Fig. 6, the maximal temperature difference between T1 and T4 for LR-4 reached around 54 °C. While the largest temperature difference for all the Cu MFEC structures were less than 5 °C. In addition, it took longer time for the packed bed to reach steady state. Fig. 7 shows that the time required to reach steady state was around 24 h for all Cu MFEC structures, and more than 40 h for the same size packed bed to reach the target CO conversion with 5.0% variation. Therefore, Cu MFEC structure possessed many obvious advantages compared with the traditional packed bed.

3.2. Product distribution

The product distributions of six major experiments were listed in Fig. 8. As shown in Fig. 8, the hybrid catalyst Fe-FTS/ZSM-5 significantly reduced C_{21}+ selectivity and increased the selectivities to lighter hydrocarbons including CH_4 and C_2–C_4. This is attributed to the deep hydrocracking activity of ZSM-5. As hybrid catalyst Fe-FTS/ZSM-5 did, hybrid catalyst Fe-FTS/MAS further increased the selectivities of light hydrocarbons (CH_4 and C_2–C_4) and greatly reduced the liquid products (C_5–C_{20}) selectivity and wax (C_{21}+) selectivity. This is mainly because MAS has a larger pore size (3.5 nm) than ZSM-5 (0.56 nm), so long chain hydrocarbons can access the internal surface of MAS and resulted in over hydrocracking. Hybrid catalyst Fe-FTS/Pt-MAS with bifunctional catalyst Pt-MAS increased the production of liquid products by suppressing the formation of C_1, C_2–C_4 and CO_2. This bifunctional catalyst

Please cite this article in press as: X. Cheng, et al., Microfibrous entrapped hybrid iron-based catalysts for Fischer–Tropsch synthesis, Catal. Today (2016), http://dx.doi.org/10.1016/j.cattod.2016.02.048

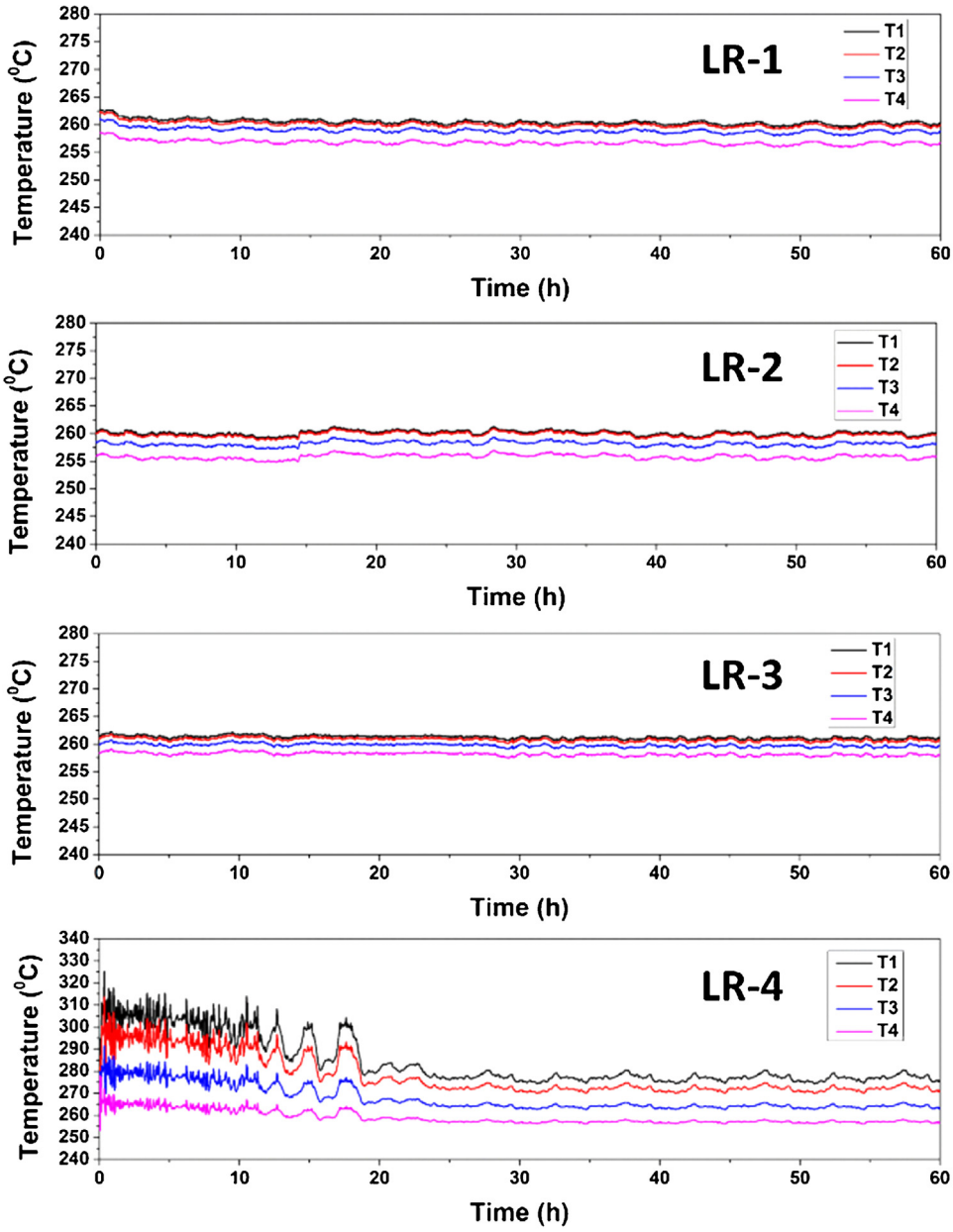

Fig. 6. Temperature profiles of four experiments in the large reactor: LR-1, LR-2, and LR-3 are Cu MFEC structures; LR-4 is a packed bed diluted with α-Al_2O_3 (T1 to T4 are radial temperature points started from centerline and the intervals between each point are 10.0 mm, 2.0 mm and 5.0 mm, respectively.).

(Pt-MAS) consisting of noble metal Pt which is responsible for hydrogenation/dehydrogenation reactions, and the support MAS, whose acid sites are responsible for activation of C—C and C—H bonds via a carbocationic mechanism. A proper balance between acid sites strength and hydrogenation/dehydrogenation activity could lead to moderate cracking and maximize the formation of liquid products [50,52].

LR-1 was carried out in the presence of thermally conductive copper microfibrous network and at the same experimental conditions used for SR-1. Fig. 8 shown that LR-1 had a similar product distribution pattern with SR-1. This fact confirmed that MFEC approach can successfully remove the heat generated inside the 34.0 mm I.D reactor and provide a uniform temperature pro-file as a packed bed reactor of 9.5 mm I.D. (SR-1) did. Similarly, LR-3 was used to compare SR-4. Results shown in Fig. 8 suggest that they have a similar product distribution pattern except the selectivity of C_2–C_4 in the MFEC reactor was slightly higher than in the packed bed reactor in SR-4, but the liquid product (C_5–C_{20}) selectivity still at a similar level. In short, the MFEC approach enabled FTS and bifunctional hydrocracking to take place simultaneously in a single reactor and provide efficient thermal management for both reactions in a fixed bed reactor with a large reactor diameter.

3.3. Olefin selectivity

The olefin content in carbon number fractions for gas phase products is shown in Fig. 9. It is shown that SR-1 demonstrated a very high olefin yield because of the relatively low tendency of secondary reactions for alkali-promoted iron-based catalysts. Moreover, the olefin content of SR-1 gradually declined with chain length, which is a typical phenomenon for Fe-based catalyst [38,53,54]. LR-1 demonstrated a similar olefin content with SR-1, which is another evidence to prove the MFEC approach is very successful for FTS in larger diameter reactor. Compared with

Please cite this article in press as: X. Cheng, et al., Microfibrous entrapped hybrid iron-based catalysts for Fischer–Tropsch synthesis, Catal. Today (2016), http://dx.doi.org/10.1016/j.cattod.2016.02.048

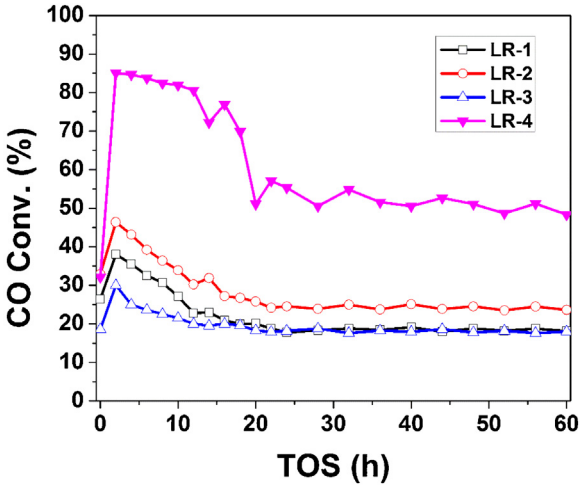

Fig. 7. CO conversion vs. time on stream for four experiments operated in the large reactor: LR-1 and LR-2 for Fe-FTS; LR-3 for Fe-FTS/Pt-MAS (empty dot for Cu MFEC structure); LR-4 for Fe-FTS (solid dot for packed bed).

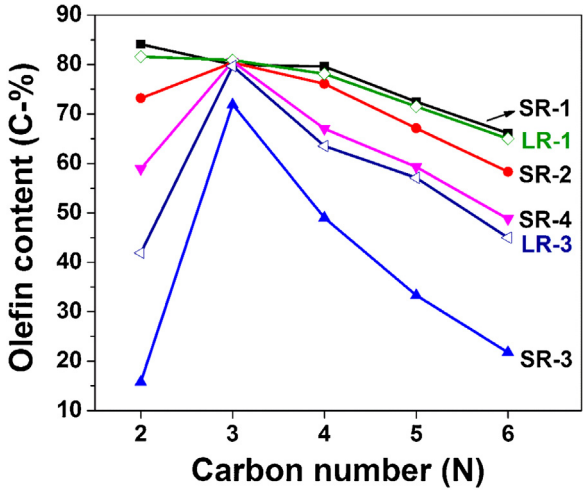

Fig. 9. Olefin content of light hydrocarbons for experiments operated in the small reactor (SR-1 to SR-4, solid dot) and in the large reactor (LR-1 and LR-3, empty dot): SR-1 for Fe-FTS; SR-2 for Fe-FTS/ZSM-5; SR-3 for Fe-FTS/MAS; SR-4 for Fe-FTS/Pt-MAS; LR-1 for Fe-FTS with Cu MFEC structure; LR-3 for Fe-FTS/Pt-MAS with Cu MFEC structure.

plain FTS catalyst in SR-1, the hybrid catalysts (SR-2, SR-3, and SR-4) demonstrated lower olefin content. This is because the hydrocracking catalysts provided active protons to terminate the active olefin components. The olefin content of SR-4 is higher than that of SR-3, due to the dehydrogenation effect of noble metal Pt. The LR-3 is a MFEC counterpart of SR-4. The result in Fig. 8 shows that the olefin content of LR-3 was slightly lower than SR-4. As mentioned above, the space velocity of LR-3 was decreased in order to increase the CO conversion to a comparable level with SR-4. Therefore, the lower olefin content in LR-3 is probably caused by the lower space velocity of LR-3, which is also consistent with the literature observations [38,55].

4. Conclusion

The Cu MFEC structure was evaluated for FTS using a highly active and stable iron-based Fischer–Tropsch synthesis catalyst (Fe-FTS) and various highly active hybrid FTS catalysts. At a CO conversion of 27.7%, the apparent reaction rate constant of Fe-FTS reached 167 mmol $(H_2 + CO)/g_{cat}/h$, and the catalyst productivity of Fe-FTS was 0.30 $gC_5+/g_{cat}/h$, which are comparable to those of the most active unsupported Fe-based catalyst. The hybrid catalyst of Fe-FTS and a bifunctional hydrocracking catalyst, i.e. Pt-MAS demonstrated FTS and hydrocracking activities simultaneously. Compared with Fe-FTS, the hybrid catalyst demonstrated low CO_2 selectivity of 27.7 C% and high C_5–C_{20} selectivity of 38.1 C%. In addition, MFEC approach enabled FTS carried out in a larger tubular reactor (34.0 mm I.D.) without comprising the production rate and selectivity to desired product. The maximum temperature difference along the radial direction was less than 5 °C for all the MFEC structures, while the temperature difference for the packed bed tested under the same condition was around 54 °C. Moreover, a steady state for the Cu MFEC structure can be reached rapidly compared with packed bed of the same size. In conclusion, the Cu MFEC approach provides a superior thermal management for FTS reaction and it enables FTS process intensification. When combined with the hybrid catalyst approach, Cu MFEC approach may provide a unique opportunity to utilize Gas-to-Liquids economically even at small scales.

Acknowledgement

This work was supported by IntraMicron Inc. under a contact G00007979.

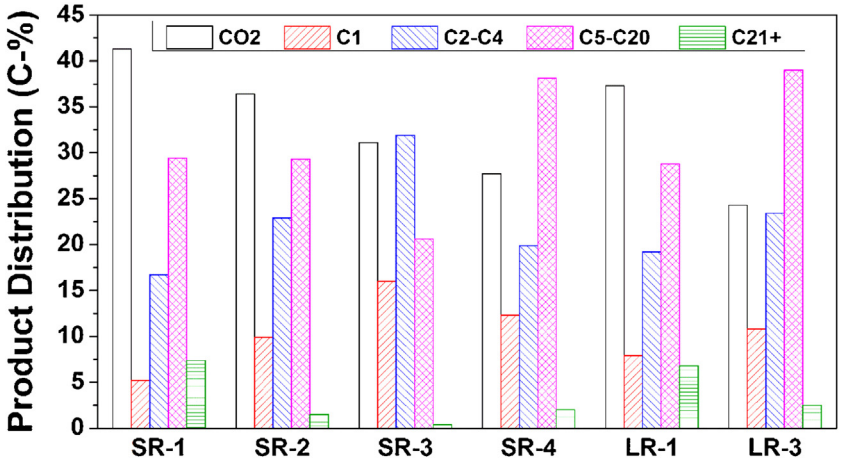

Fig. 8. Product distribution of the experiments operated both in the small reactor (SR-1 to SR-4) and in the large reactor (LR-1 and LR-3): SR-1 for Fe-FTS; SR-2 for Fe-FTS/ZSM-5; SR-3 for Fe-FTS/MAS; SR-4 for Fe-FTS/Pt-MAS; LR-1 for Fe-FTS with Cu MFEC structure; LR-3 for Fe-FTS/Pt-MAS with Cu MFEC structure.

Please cite this article in press as: X. Cheng, et al., Microfibrous entrapped hybrid iron-based catalysts for Fischer–Tropsch synthesis, Catal. Today (2016), http://dx.doi.org/10.1016/j.cattod.2016.02.048

Appendix A. Supplementary data

Supplementary data associated with this article can be found, in the online version, at http://dx.doi.org/10.1016/j.cattod.2016.02.048.

References

[1] E.F. Sousa-Aguiar, F.B. Noronha, A. Faro Jr., Catal. Sci. Technol. 1 (2011) 698–713.
[2] B.H. Davis, Top. Catal. 32 (2005) 143–168.
[3] R.M. De Deugd, F. Kapteijn, J.A. Moulijn, Top. Catal. 26 (2003) 29–39.
[4] D.J. Duvenhage, T. Shingles, Catal. Today 71 (2002) 301–305.
[5] M.E. Dry, Catal. Today 71 (2002) 227–241.
[6] S.T. Sie, R. Krishna, Appl. Catal. A Gen. 186 (1999) 55–70.
[7] R.L. Espinoza, A.P. Steynberg, B. Jager, A.C. Vosloo, Appl. Catal. A Gen. 186 (1999) 13–26.
[8] W. Liu, J. Hu, Y. Wang, Catal. Today 140 (2009) 142–148.
[9] A.M. Hilmen, E. Bergene, O.A. Lindvåg, D. Schanke, S. Eri, A. Holmen, Catal. Today 69 (2001) 227–232.
[10] R.M. De Deugd, F. Kapteijn, J.A. Moulijn, Catal. Today 79–80 (2003) 495–501.
[11] L.C. Almeida, F.J. Echave, O. Sanz, M.A. Centeno, G. Arzamendi, L.M. Gandía, E.F. Sousa-Aguiar, J.A. Odriozola, M. Montes, Chem. Eng. J. 167 (2011) 536–544.
[12] J.C. Park, N.S. Roh, D.H. Chun, H. Jung, J.I. Yang, Fuel Process. Technol. 119 (2014) 60–66.
[13] C. Maretto, R. Krishna, Catal. Today 66 (2001) 241–248.
[14] E. Tronconi, G. Groppi, T. Boger, A. Heibel, Chem. Eng. Sci. 59 (2004) 4941–4949.
[15] L. Giani, G. Groppi, E. Tronconi, Ind. Eng. Chem. Res. 44 (2005) 4993–5002.
[16] D.K. Harris, D.R. Cahela, B.J. Tatarchuk, Compos. Part A Appl. Sci. Manuf. 32 (2001) 1117–1126.
[17] D.R. Cahela, B.J. Tatarchuk, Catal. Today 69 (2001) 33–39.
[18] L.L. Murrell, F.M. Dautzenberg, R.A. Overbeek, B.J. Tatarchuk, US Patent 20020068026, June 6, 2002.
[19] B. Tatarchuk, H. Yang, R. Kalluri, D. Cahela, US Patent 8420023, April 16, 2013.
[20] B.J. Tatarchuk, B.K. Chang, Y. Lu, L. Chen, E. Luna, D. Cahela, US Patent 7501012, March 10, 2009.
[21] H. Yang, B.J. Tatarchuk, T.J. Barron, P.S. Dimick, US Patent 20150236386, August 20, 2015.
[22] H. Yang, P.S. Dimick, T.J. Barron, B.J. Tatarchuk, US Patent 20150176894, June 25, 2015.
[23] D.R. Cahela, B.J. Tatarchuk, Ind. Eng. Chem. Res. 53 (2014) 6509–6520.
[24] H. Yang, Y. Lu, B.J. Tatarchuk, J. Power Sources 174 (2007) 302–311.
[25] H. Yang, D.R. Cahela, B.J. Tatarchuk, Chem. Eng. Sci. 63 (2008) 2707–2716.
[26] W.H. Zhu, P.J. Durben, B.J. Tatarchuk, J. Power Sources 111 (2002) 221–231.
[27] W.H. Zhu, M.E. Flanzer, B.J. Tatarchuk, J. Power Sources 112 (2002) 353–366.
[28] Q. Gu, R.T. Henderson, B.J. Tatarchuk, Eng. Appl. Comput. Fluid Mech. 9 (2015) 567–576.
[29] M. Sheng, D.R. Cahela, H.Y. Yang, C.F. Gonzalez, W.R. Yantz, D.K. Harris, B.J. Tatarchuk, Int. J. Heat Mass Transf. 56 (2013) 10–19.
[30] M. Sheng, H. Yang, D.R. Cahela, B.J. Tatarchuk, J. Catal. 281 (2011) 254–262.
[31] M. Sheng, H. Yang, D.R. Cahela, W.R. Yantz, C.F. Gonzalez, B.J. Tatarchuk, Appl. Catal. A Gen. 445–446 (2012) 143–152.
[32] H. Schulz, Catal. Today 178 (2011) 151–156.
[33] S. Zhang, R. Xu, E. Durham, C.B. Roberts, AIChE J. 60 (2014) 2573–2583.
[34] Y. Yoneyama, J. He, Y. Morii, S. Azuma, N. Tsubaki, Catal. Today 104 (2005) 37–40.
[35] C. Kibby, K. Jothimurugesan, T. Das, H.S. Lacheen, T. Rea, R.J. Saxton, Catal. Today 215 (2013) 131–141.
[36] S. Sartipi, M. Makkee, F. Kapteijn, J. Gascon, Catal. Sci. Technol. 4 (2014) 893–907.
[37] H. Schulz, Appl. Catal. A Gen. 186 (1999) 3–12.
[38] G.P. van der Laan, A.A.C.M. Beenackers, Catal. Rev. Sci. Eng. 41 (1999) 255–318.
[39] K. Keyvanloo, M.K. Mardkhe, T.M. Alam, C.H. Bartholomew, B.F. Woodfield, W.C. Hecker, ACS Catal. 4 (2014) 1071–1077.
[40] C.L. Kibby, K. Jothimurugesan, T.K. Das, R.J. Saxton, A.W. Burton, US Patent 7943674, May 17, 2011.
[41] K. Keyvanloo, J.B. Horton, W.C. Hecker, M.D. Argyle, Catal. Sci. Technol. 4 (2014) 4289–4300.
[42] Y. Zhang, X. Shi, J.M. Kim, D. Wu, Y. Sun, S. Peng, Catal. Today. 93–95 (2004) 615–618.
[43] D.B. Bukur, X. Lang, Ind. Eng. Chem. Res. 38 (1999) 3270–3275.
[44] D.B. Bukur, X. Lang, D. Mukesh, W.H. Zimmerman, M.P. Rosynek, C. Li, Ind. Eng. Chem. Res. 29 (1990) 1588–1599.
[45] E.F. Iliopoulou, S.D. Stefanidis, K.G. Kalogiannis, A. Delimitis, A.A. Lappas, K.S. Triantafyllidis, Appl. Catal. B Environ. 127 (2012) 281–290.
[46] V.M. Akhmedov, S.H. Al-Khowaiter, Catal. Rev. 49 (2007) 33–139.
[47] M. Baranak, B. Gürünlü, A. Sarıoğlan, Ö. Ataç, H. Atakül, Catal. Today 207 (2013) 57–64.
[48] F.A.N. Fernandes, Chem. Eng. Technol. 28 (2005) 930–938.
[49] S. Gamba, L.A. Pellegrini, V. Calemma, C. Gambaro, Catal. Today 156 (2010) 58–64.
[50] C. Bouchy, G. Hastoy, E. Guillon, J.A. Martens, Oil Gas Sci. Technol. 64 (2009) 91–112.
[51] W. Yu, B. Wu, J. Xu, Z. Tao, H. Xiang, Y. Li, Catal. Lett. 125 (2008) 116–122.
[52] V.M. Akhmedov, S.H. Al-Khowaiter, Catal. Rev. Sci. Eng. 44 (2002) 455–498.
[53] H. Schulz, Catal. Today 228 (2014) 113–122.
[54] H. Schulz, Catal. Today 214 (2013) 140–151.
[55] E. Iglesia, S.C. Reyes, R.J. Madon, J. Catal. 129 (1991) 238–256.

Please cite this article in press as: X. Cheng, et al., Microfibrous entrapped hybrid iron-based catalysts for Fischer–Tropsch synthesis, Catal. Today (2016), http://dx.doi.org/10.1016/j.cattod.2016.02.048